AUT Journal of Mechanical Engineering

AUT J. Mech. Eng., 1(1) (2017) 3-12
DOI: 10.22060/mej.2016.715

Investigation of Mixed Electro-Osmotic/Poiseuille Slip Flows of Viscoelastic Fluids in Rectangular Microchannels with Hydrophobic Surfaces

M. Reshadi, M. H. Saidi*

Mechanical Engineering Department, Center of Excellence in Energy Conversion (CEEC), Sharif University of Technology, Tehran, Iran

ABSTRACT: In this paper, we conduct a numerical study of mixed electro-osmotic/Poiseuille slip flows of viscoelastic fluids in microchannels with rectangular cross sections by means of second order finite difference method. In this regard, the complete form of the PTT-constitutive equation is used to describe the rheological behavior of the fluid. The numerical results being validated by the same simplified theoretical study reveal an excellent accuracy with relative error less than 0.3%. Afterward, the extended numerical study is used to investigate the 2D velocity distribution and volumetric flow rate in the presence of wall surface hydrophobicity through rectangular microchannels. In addition, in this investigation, the exact solution of unidirectional electroosmotic flow of PTT-viscoelastic fluids is derived for slit hydrophobic microchannels, and after validating, the solution is used to investigate the rheological behavior of viscoelastic fluids in the range of operating parameters. The results exhibit a uniform effect of hydrophobicity in increasing the profile of 1D velocity distribution in slit microchannels. Finally, in order to determine the stability of the grid network, various under relaxation factors are applied to determine the speed of convergence of finite difference method, and then, by using the analytical procedure, the critical Weissenberg number is introduced as a function of velocity scale ratio and Debye–Hückel parameter. The evaluation of the numerical method in the critical area indicates the stability of viscoelastic fluid flow for the values of the Weissenberg number less than the corresponding critical value in the theoretical analysis.

Review History:

Received: 23 November 2015
Revised: 12 February 2016
Accepted: 11 April 2016
Available Online: 8 November 2016

Keywords:

Electro-osmosis
Viscoelasticity
Hydrophobicity
Microfluidics

1- Introduction

The development of microfluidic devices produced and formed by hydrophobic materials for diagnostic techniques and biomedical analysis has led to some inaccuracies of conventional methods of flow modeling against experimental data. Some of these unconformities are due to considering no-slip boundary conditions in analyzing the flow behavior through these micro-geometries [1]. In the case of macro-scale geometries, the no-slip boundary conditions for Newtonian fluid flows match well with the macroscopic experimental data. However, some experimental results showed the inaccuracy of such boundary conditions for non-Newtonian fluid flows over the hydrophobic surfaces [2-4]. In the recent years, the extension of these investigations to the cases of electroosmotic flow [5, 6], micro-total analysis systems [7, 8], biological assays in microchannels [9, 10], and gaseous micro-flows [11] has been carried out by some researchers, and the related results have revealed some deviations from conventional mathematical modeling of flow analysis for Newtonian fluid flows through microscopic geometries and microchannels [12, 13].

In the last decade, the electroosmotic mechanism has been widely used in the field of biological and chemical assays such as enzyme reaction [14], protein folding [15], synthesis or reaction of chemical compounds [16, 17], etc. Meanwhile, hydrophobic properties of some materials have gained enormous importance for fabrication of Lab-On-a-Chip (LOC) devices, and such hydrophobic surfaces have presented an efficient way to viscous drag reduction at the fluid-solid interface in these microsystems [18,19]. In this regard, Soong et al. [14] and Jamaati et al. [15] have reported some analytical studies for the simulations of electroosmotic flow of Newtonian fluids through microchannels with hydrophobic surfaces. In these studies, the Navier slip boundary condition is considered as an effective approach to properly model the existence of slippage between the fluid and walls of the microchannel [16]. On the other hand, the investigation of Tretheway and Meinhart [17] revealed that the hydrodynamic characteristics of slip flows depends on the kind of the fluid and hydrophobic properties of channel wall surface. As the microfluidic channels are commonly fabricated by soft lithography technique [18] using polydimethylsiloxane (PDMS), accordingly, the amount of slippage in the solid wall-fluid interface may depend on the kind of the fluid in contact with such hydrophobic surfaces.

In the recent analytical studies which has been conducted in the field of electroosmotic flow, the hydrodynamic characteristics of pressure driven electrokinetic slip flows of viscoelastic fluids in planar microfluidic channels with hydrophobic surfaces were investigated, and the simplified Phan-Thien-Tanner (PTT) model was used as the constitutive equation of the fluid [1]. Since in most cases, the microchannels are produced in rectangular cross sections with finite aspect ratios, one of the main issues, which has remained open to discussion, is to quantify the effect of sidewalls of the microchannel in velocity distribution. Closely related to this question, this research aims to evaluate this effect by means of 2D analysis of the combined electroosmotic and pressure-driven flow of viscoelastic fluids with finite difference method. The complete form of PTT model [19, 20] with the Gordon–Schowalter convected derivative, which covers the upper convected Maxwell, Johnson-Segalman and FENE-P models, describes the rheological behavior of the fluid. In our numerical approach, we proceed to solve the governing equations of the problem, including the non-linear Poisson–

Corresponding author, E-mail: saman@sharif.edu

Boltzmann (PB), momentum and the constitutive equation of PTT model in a two-dimensional fashion. Also in this paper, by considering the complete form of PTT model, we extend the previous analytical solutions to analyze the electroosmotic flow of viscoelastic fluids in planar microchannels with hydrophobic surfaces and symmetric wall zeta potentials, and then, with the aid of the obtained 1D velocity profile, the rheological behavior of viscoelastic fluids under various fluid-wall slippage conditions is investigated. Moreover, the effect of Navier slip coefficient and slip exponent on the volumetric flow rate is studied.

2- Mathematical modeling of the problem

Fig. 1a schematically illustrates the flow of viscoelastic fluid under the combined effect of electroosmotic and pressure driving forces through a microchannel with rectangular cross-section. In Fig. 1b, the formation of the electric double layer near the dielectric walls of the microchannel with negative zeta potential is depicted. As shown, due to the accumulation of positive ions near the walls because of electrolyte-wall ion interaction, a thin immobile layer of positively charged ions (Stern layer) is established in this region. Closely near this layer, a mobile layer containing net positive charges with lower density is formed which by applying an external electric field by means of an anode and cathode shown in Fig. 1a, the net flux motion of ions in this layer is generated. The movement of counter-ions in diffuse layer causes to exert a drag force to the carrier fluid, and consequently, the electroosmotic flow emerges in the axial direction of the microchannel. Fig. 1b also shows the grid network for the numerical simulation in which by using a logarithmic relation introduced in section 4, the grid clustering in the vicinity of the channel walls is produced.

We make the following assumptions in modeling and simplifying the present problem:

1. The flow is considered to be steady, fully developed and incompressible with the Reynolds number less than unity, i.e., $Re<1$.
2. The concentration of ions is high enough which allows neglecting the EDL overlap in the center of microchannel [21].
3. The axial length of the microchannel is much larger than the size of the channel cross section, i.e., $L >> H, W$, for which, the hydrodynamic entrance length can be ignored.
4. The electrokinetic properties of the interfacial fluid-wall are considered independent of the slip boundary conditions.
5. All thermo-physical properties of the viscoelastic fluid are considered constant and independent of temperature.

3- Governing equations

In this section, the governing equations of the problem in the Cartesian coordinate as shown in Fig. 1 are introduced. These equations for a fully developed, incompressible PTT-viscoelastic flow are the Poisson–Boltzmann equation, the equation of continuity, and the modified momentum equation coupled with the constitutive equation of PTT model governing the extra polymeric stress tensor, which are respectively written as follows:

$$\nabla^2\bar{\psi} = \mathrm{K}^2\sinh\bar{\psi} \tag{1}$$

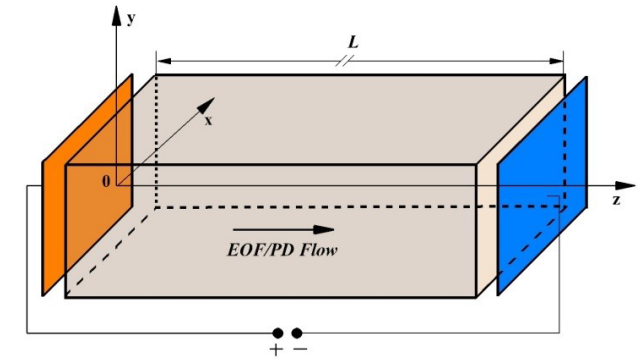

(a)

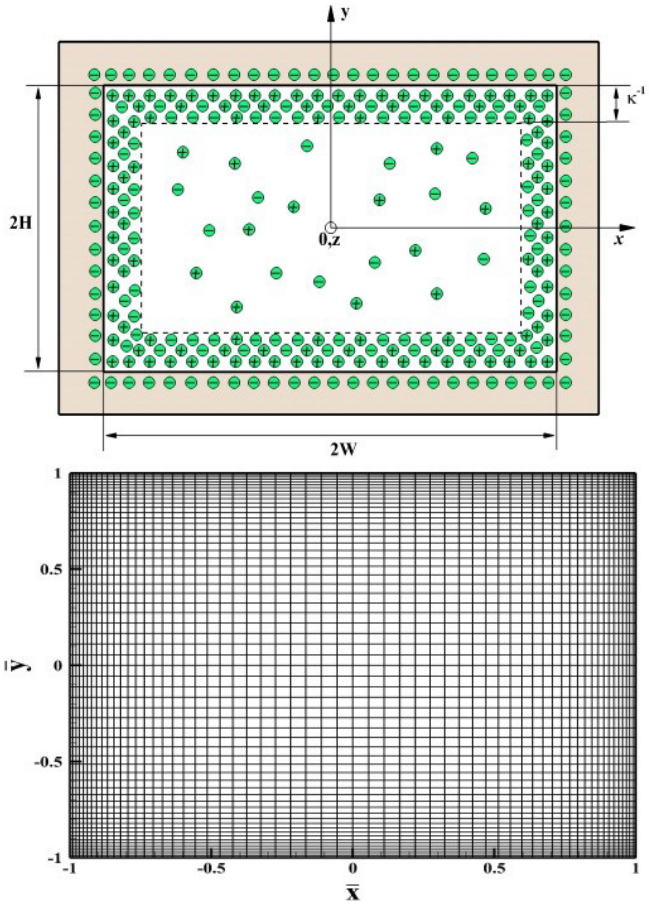

(b)

Fig. 1. Schematic of mixed electroosmotic and pressure driven flows in rectangular microchannel (a) axial length of channel, including cathode and anode, (b) cross section of microchannel, including EDL formation and computational network

$$\nabla.\bar{\boldsymbol{u}} = 0 \tag{2}$$

$$\nabla.\bar{\tau} = \frac{\Gamma}{K} - \frac{K}{\bar{\psi}_0}\sinh\bar{\psi} \tag{3}$$

$$f\left(\bar{\tau}_{kk}\right)\bar{\tau} + \frac{\mathrm{We}_\kappa}{K}\left\{-\bar{\tau}.\bar{\nabla}\bar{\boldsymbol{u}} - \bar{\nabla}\bar{\boldsymbol{u}}^T.\bar{\tau} + \frac{\xi}{2}\left[\left(\bar{\nabla}\bar{\boldsymbol{u}} + \bar{\nabla}\bar{\boldsymbol{u}}^T\right).\bar{\tau} + \bar{\tau}.\left(\bar{\nabla}\bar{\boldsymbol{u}} + \bar{\nabla}\bar{\boldsymbol{u}}^T\right)\right]\right\} = \bar{\nabla}\bar{\boldsymbol{u}} + \bar{\nabla}\bar{\boldsymbol{u}}^T \tag{4}$$

where in the above equations, the quantities with dashed superscript indicate the dimensionless form of the corresponding variables in the present problem. The characteristics of length and velocity for non-dimensionalization of the problem variables are half the channel height (H) and Helmholtz–Smoluchowski velocity [21] defined as $u_{HS}=-\epsilon\psi_0 E_z/\eta_p$, respectively. In this way, the dimensionless parameters are stated as follows:

$$\bar{x}=\frac{x}{H},\bar{y}=\frac{y}{H},\alpha=\frac{W}{H},K=\kappa H$$
$$\bar{\psi}=\frac{e\mathbb{Z}\psi}{k_BT_m},\bar{\psi}_0=\frac{e\mathbb{Z}\psi_0}{k_BT_m},\bar{u}=\frac{u}{u_{HS}} \quad (5)$$
$$\Gamma=-\frac{H^2P_z}{\epsilon\psi_0E_z},\bar{\tau}=\frac{\tau}{\eta_p u_{HS}\kappa},\mathrm{We}_\kappa=\lambda u_{HS}\kappa$$

where $K=\kappa H$ is the dimensionless Debye–Hückel parameter in which $\kappa=(2n_0e^2z^2/\epsilon k_BT_m)^{1/2}$. In these formulations, We_κ is the Weissenberg number based on the Debye length characterizing the extent of elasticity of the fluid. In addition, $f(\bar{\tau}_{kk})=1+\varepsilon We_\kappa(\bar{\tau}_{xx}+\bar{\tau}_{yy}+\bar{\tau}_{zz})$ is the linear form of the stress coefficient function proposed by Phan-Thien and Tanner [19,20]. The other parameters are introduced in the Nomenclature, and for the sake of saving space are not explained here.

4- Boundary conditions and numerical analysis

The boundary condition for electrical potential distribution is the zeta potential of the wall and for the velocity distribution is the general non-linear form of the Navier slip relation. In addition, for both electrical potential and velocity profiles, the symmetry conditions at the channel main axes are considered in the numerical simulation. Therefore, the relevant computations are performed in the right upper quadrant of the channel cross section. Following the above statements, the boundary condition can be written as:

$$\bar{\psi}\big|_{\bar{x}=\alpha}=\bar{\psi}\big|_{\bar{y}=1}=\bar{\psi}_0$$
$$\bar{u}\big|_{\bar{x}=\alpha}=-\bar{L}_s\left(\bar{\tau}_{xz}\big|_{\bar{x}=\alpha}\right)^m$$
$$\bar{u}\big|_{\bar{y}=1}=-\bar{L}_s\left(\bar{\tau}_{yz}\big|_{\bar{y}=1}\right)^m \quad (6)$$
$$\left.\frac{\partial\bar{\psi}}{\partial\bar{x}}\right|_{\bar{x}=0}=\left.\frac{\partial\bar{\psi}}{\partial\bar{y}}\right|_{\bar{y}=0}=\left.\frac{\partial\bar{u}}{\partial\bar{x}}\right|_{\bar{x}=0}=\left.\frac{\partial\bar{u}}{\partial\bar{y}}\right|_{\bar{y}=0}=0$$

where $\bar{L}_s=L_s(\eta_p\kappa)^m u_{HS}^{m-1}$ is the dimensionless form of the Navier slip coefficient, L_s, and m is the slip exponent which is in the range of 1 to 4 [22]. Therefore, based on the above boundary conditions, the solution of the Eqs. (1-4) can be obtained numerically. In this state, to enhance the quality and resolution of the results, and also, decrease the amount of numerical diffusion stemming from the truncation errors in the second order approximation of the derivatives in the governing equations, we use a refined grid network, in which, the grid points are clustered near the walls of the microchannel where there is a sharp variation of velocity and electrical potential in these regions. Thus, in order to cluster the grids in the physical plane $(\bar{x},\bar{y})$ and transform it to the computational plane $(\hat{x},\hat{y})$ we use the following relations between these two spaces [23]:

$$\hat{x}=\frac{1}{\Omega}\ln\left(\frac{\beta+\bar{x}/\alpha}{\beta-\bar{x}/\alpha}\right) \quad (7)$$

$$\hat{y}=\frac{1}{\Omega}\ln\left[(\beta+\bar{y})/(\beta-\bar{y})\right] \quad (8)$$

where $\Omega=\ln((\beta+1)/(\beta-1))$ in which β is the stretching parameter in the transverse direction, such that by approaching β to unity, the amount of clustering the grids near the walls increase. Then, by transforming the governing equations (1-3) into the computational plane, and afterwards, discretizing them by a second order central difference method in the $(\hat{x},\hat{y})$ space, the algebraic form of these equations can be obtained, respectively, as follows:

$$A_{\psi_p}\bar{\psi}_p=\sum_{i=1}^{4}A_{\psi_i}\bar{\psi}_{NB_i} \quad (9)$$

$$A_{u_p}\bar{u}_p=\sum_{i=1}^{4}A_{u_i}\bar{u}_{NB_i}+A_{u_c} \quad (10)$$

where A_ψ and A_u are the coefficients of the discretized form of the electrical potential and momentum equations, respectively, and A_{u_c} is the discretized source term of the momentum equation containing the electroosmotic and pressure driving forces in the channel axial direction. The indices P and NB refer to the central node and neighbor grid points in vertical and horizontal directions, respectively. Finally, the Gauss-Seidel iteration method is employed for solving the above system of linear algebraic equations and the iterative procedure in this algorithm is continued until the specified overall relative error of 10^{-8} for the electrical potential and velocity between two successive iterations is obtained.

5- Exact solution of velocity profile in microchannels with large aspect ratios

For rectangular microchannels with a large aspect ratio of the cross-section, i.e., $\alpha=W/H>>1$, it is demonstrated that the effect of channel side-walls on the flow dynamics can be ignored with sufficient accuracy [21]. In Fig. 2a, the diagram of a slit microchannel with the aforementioned properties are schematically illustrated. In accordance with section 2, the walls of the microchannel have a negative zeta potential, and accordingly, due to the absorption of cations of the electrolyte solution (blue circles in Fig. 2a) at the vicinity of the channel walls, the EDL is formed in these regions (see Fig. 2b). For this case, the governing equations of the present viscoelastic fluid flow problem (1-4) can be written in one-dimensional fashion through which the terms depending on the x direction are neglected. At first, the one-dimensional form of the Poisson-Boltzmann equation, i.e., Eq. (1), as the governing equation of electrical potential distribution together with the associated boundary conditions can be written as follows:

$$\begin{cases}\dfrac{d^2\bar{\psi}}{d\bar{y}^2}=\mathrm{K}^2\sinh\bar{\psi}\approx\mathrm{K}^2\bar{\psi}\\[2ex]\left.\dfrac{d\bar{\psi}}{d\bar{y}}\right|_{\bar{y}=0}=0\ ,\ \bar{\psi}\big|_{\bar{y}=1}=\bar{\psi}_0\end{cases} \quad (11)$$

where considering the conditions of the standard electrokinetic model and $\psi_0\le 25$ mV at the room temperature, the Debye–Hückel approximation can be used to linearize the non-homogeneous term of the above equation. Also, it is noted that the symmetry boundary conditions and the equality with

zeta potential at the channel walls are used as the boundary conditions for the electrical potential distribution. Therefore, the analytical solution of the above differential equation can be written as:

$$\bar{\psi} = \bar{\psi}_0 \frac{\cosh\left(K\bar{y}\right)}{\cosh K} \tag{12}$$

Afterward, the one-dimensional form of the PTT constitutive equation (Eq. (4)) is employed, and by dropping terms depending on the x direction, the remaining stress components can be extracted from this equation as follows:

$$\bar{\tau}_{yy} = -\frac{\xi}{f}\frac{\mathrm{We}_{\hat{\epsilon}}}{K}\bar{\tau}_{yz}\bar{u}_y \tag{13}$$

$$\bar{\tau}_{zz} = -\frac{\xi-2}{f}\frac{\mathrm{We}_{\hat{\epsilon}}}{K}\bar{\tau}_{yz}\bar{u}_y \tag{14}$$

$$\bar{\tau}_{yz} = \frac{\bar{u}_y}{f}\left\{\frac{\mathrm{We}_{\kappa}}{K}\left[\left(1-\frac{\xi}{2}\right)\bar{\tau}_{yy} - \frac{\xi}{2}\bar{\tau}_{zz}\right]+1\right\} \tag{15}$$

In order to obtain the explicit form of the $f(\bar{\tau}_{kk})$ in terms of the normal stress component in the z direction, i.e., $\bar{\tau}_{zz}$, Eq. (14) is divided by Eq. (13), by which the following relation can be obtained between the normal stress components in the y and z directions:

$$\bar{\tau}_{yy} = -\frac{\xi}{2-\xi}\bar{\tau}_{zz} \tag{16}$$

In this step, with the aid of the above equation, the linear stress coefficient function $f(\bar{\tau}_{kk})$, can be explicitly stated in terms of $\bar{\tau}_{zz}$ as follows:

$$f\left(\bar{\tau}_{kk}\right) = 1 + 2\xi\frac{\mathrm{We}_{\kappa}}{K\chi}\bar{\tau}_{zz} \tag{17}$$

where, in this equation, $\chi=\xi(2-\xi)/\varepsilon(1-\xi)$. Then, by substituting the linear stress coefficient function from Eq. (17) into Eqs. (13-15), the implicit relations between the stress components are obtained. To obtain a relation between the shear and normal stress components, we divide Eq. (15) by Eq. (14) and the following relation can be found between $\bar{\tau}_{zz}$ and $\bar{\tau}_{yz}$:

$$\xi\mathrm{We}_{\kappa}\bar{\tau}_{zz}^{\,2} - \frac{1}{3}\bar{\tau}_{zz} + \mathrm{We}_{\kappa}\left(2-\xi\right)\bar{\tau}_{yz}^{\,2} = 0 \tag{18}$$

The solution of the above quadratic equation for $\bar{\tau}_{zz}$ with respect to $\bar{\tau}_{yz}$ can be written as follows:

$$\bar{\tau}_{zz} = \frac{1}{2\xi\mathrm{We}_{\kappa}}\left(1-\sqrt{1-a^2\mathrm{We}_{\kappa}^2\bar{\tau}_{yz}^{\,2}}\right) \tag{19}$$

where $a^2=4\xi(2-\xi)$. Then, in order to analyze the continuity and momentum equations (Eqs. (2-3)) along with omitting the components depending on the x direction and using the Debye–Hückel approximation for mixed electroosmotic/ Poiseuille flows, the following differential equations can be obtained for the shear stress component:

$$\frac{d\bar{\tau}_{yz}}{d\bar{y}} = \frac{\Gamma}{K} - K\frac{\cosh\left(K\bar{y}\right)}{\cosh K} \tag{20}$$

By integrating the above equation with respect to the y direction, and considering this point that due to symmetry, $\bar{\tau}_{yz}$ is zero at the center of the microchannel, the following relation can be obtained for shear stress distribution:

$$\bar{\tau}_{yz}\left(\bar{y}\right) = \frac{\Gamma}{K}\bar{y} - \frac{\sinh\left(K\bar{y}\right)}{\cosh\left(K\right)} \tag{21}$$

Then, by combining Eqs. (15-17, 19, 20), and using the symmetry conditions at $\bar{y}=0$,, the following relation for the velocity gradient can be obtained:

$$\bar{u}_{\bar{y}} = \frac{-\frac{2}{\chi}\left(\frac{\Gamma}{K}\bar{y} - \frac{\sinh K\bar{y}}{\cosh K}\right)}{1-\sqrt{1-a^2\mathrm{We}_{\hat{\epsilon}}^2\left[\frac{\Gamma}{K}\bar{y} - \frac{\sinh K\bar{y}}{\cosh K}\right]^2} - \chi} \times\left[\chi+\left[1-\sqrt{1-a^2\mathrm{We}_{\hat{\epsilon}}^2\left(\frac{\Gamma}{K}\bar{y} - \frac{\sinh K\bar{y}}{\cosh K}\right)^2}\right]\right] \tag{22}$$

Therefore, the solution of the above equation can be obtained by using the nonlinear Navier slip boundary conditions for velocity distribution at $\bar{y}=1$. The latter can be stated in a dimensional fashion as follows:

$$\left|u\right|_{y=H} = \mathcal{L}_s\left|\tau_{yz}\right|_{y=H}^{m} \tag{23}$$

Subsequently, by calculating the amount of shear stress at the wall, $y=H$, from Eq. (21) and substituting the result to the above equation, the following relation for the slip velocity at the wall of the microchannel is obtained:

$$\left|\bar{u}\right|_{\bar{y}=1} = \bar{\mathcal{L}}_s\left(K\tanh\left(K\right)\right)^m \tag{24}$$

Therefore, according to the boundary conditions introduced in Eq. (24) and integrating the Eq. (22) with respect to $\bar{y}$, the solution of the velocity profile is obtained as written in Eq. (25), in which, $A=\cosh(K/aWe_k)$, $B=\cosh K$ and $C=\cosh K\bar{y}$ are

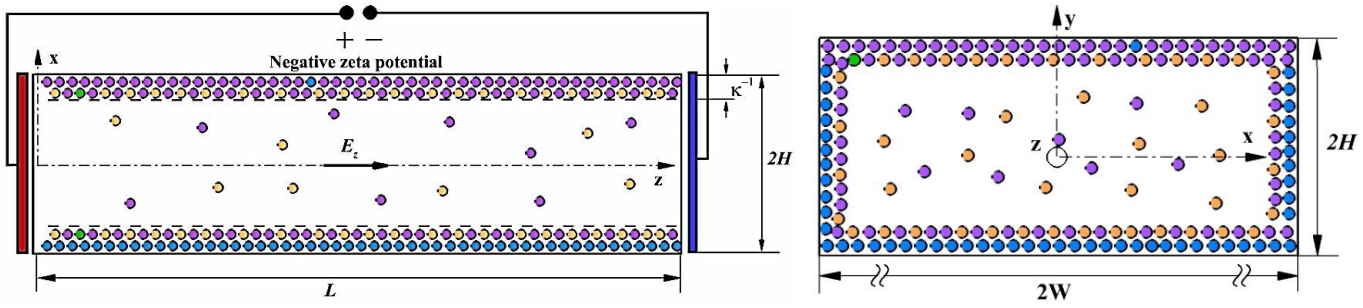

(a) (b)

Fig. 2. Schematic of electroosmotic flow in slit microchannel
(a) axial length of channel, including cathode and anode, (b) cross section of microchannel with large aspect ratios ($W>>H$)

the alternative coefficients used to compact the solution. The solution of the velocity distribution presented here covers the velocity profile for electroosmotic flow of upper convected Maxwell model, Johnson-Segalman and FENE-P model fluids in the presence of fluid-wall slippage. In comparison with previous theoretical models for electroosmotic flow of viscoelastic fluids in slit microchannels with symmetric wall zeta potentials, the present solution has the following coverage:

1. By setting $\bar{L}_s \to 0$ and $\xi \to 0$, the present velocity profile reverts to the previous analytical solution of Afonso et al. [24].
2. By removing the fluid-wall slippage for the flow of PTT fluids and setting $\bar{L}_s \to 0$, the theoretical solution of Dhinakaran et al. [25] is recovered.
3. By setting $\xi \to 0$ for the flow of sPTT fluids, the solution of Afonso et al. [1] is recovered.

6- Method validation and grid dependency study

In this section, at first, a comparison between the results of finite difference method for electroosmotic flow through microchannels with large aspect ratios and those of the analytical solution of Afonso et al. [1] in the cases of adverse and favorable pressure gradients is made. To make the comparison, in this case, we use the equivalent parameters in both studies as We_κ=15, K=20, ε=0.01, and recover the simplified form of the PTT model by setting ξ=0 in the present study. It is noteworthy that, we use a large value for channel aspect ratio (α=50) to significantly decrease the effect of side-walls on velocity distribution at the channel half-width. Then, the analytical solution of electroosmotic velocity profile in the present study is validated via the comparison with the results of the analytical solution of Dhinakaran et al. [25] in the limited case of no-slip boundary conditions. To compare the results with those of the aforementioned study, we set $\bar{L}_s \to 0$ in order to remove the fluid-wall slippage, and then, the velocity profile of the electroosmotic flow at the three cases of the Weissenberg number, We_κ=1, 3, 4 is validated.

As can be seen from Fig. 3, for the two kinds of adverse and favorable pressure gradients, two values of the Navier slip coefficient, $\bar{L}_s$=0.001, 0.0005, and two values of slip exponent m=1, 2, the results of the present 2D numerical study are in good agreement with the analytical results of Ref. [1] with the maximum relative error less than 0.3%, and therefore, the results of the present FDM simulation can be used for microchannels with various channel aspect ratios. Also, for various values of the Weissenberg number, the comparison between the analytical solution of the present study and that of Dhinakaran et al. [25] at the limited case of no-slip boundary conditions is made in Fig. 4. As is evident, both results are in a good accord again. Therefore, the present analytical solution can be utilized for electroosmotic flow of viscoelastic fluids described by the complete from of the PTT model through slit microchannels with hydrophobic wall surfaces.

In the present numerical simulation, the number of 225 thousand grid points with equal lateral and transversal space discretization of 150×150 grids is employed. The reason for selecting such number of grids in each direction are explained as follows: at first, in order to evaluate the minimum grid points to obtain grid independent results, we use the dimensionless volumetric flow rate defined as:

$$\bar{u}(\bar{y}) = \frac{2}{\chi}\left(\frac{C}{B}-1\right)+\frac{A^2}{B}\left(\frac{2+\chi}{\chi}\right) \times\left\{-\frac{2}{A}\left[\sin^{-1}\left[\frac{C\sqrt{A^2-B^2+1}-B\sqrt{A^2-C^2+1}}{1+A^2}\right]\right] +\ln\left[\left(\frac{\sqrt{A^2-B^2+1}+AB}{\sqrt{A^2-B^2+1}-AB}\right)\left(\frac{B-1}{B+1}\right)\left(\frac{\sqrt{A^2-C^2+1}-AC}{\sqrt{A^2-C^2+1}+AC}\right)\left(\frac{C+1}{C-1}\right)\right]\right\} +\frac{\bar{L}_s K^m}{B^m}\left|B^2-1\right|^{\frac{m}{2}} \tag{25}$$

where u_m is the average velocity of viscoelastic fluid flow through rectangular microchannel.

$$\bar{Q} = \frac{Q}{4HWu_{HS}} = \frac{u_m}{u_{HS}} = \int_0^1\int_0^1 \frac{\alpha^{-1}\bar{u}\,d\hat{x}\,d\hat{y}}{M_1(\bar{x})M_3(\bar{y})} \tag{26}$$

Also, $\bar{M}_1(x)$ and $\bar{M}_3(y)$ are the first derivatives of the transformed computational coordinates, $(\hat{x},\hat{y})$, with respect to their corresponding physical coordinates, $(\bar{x},\bar{y})$, in the x

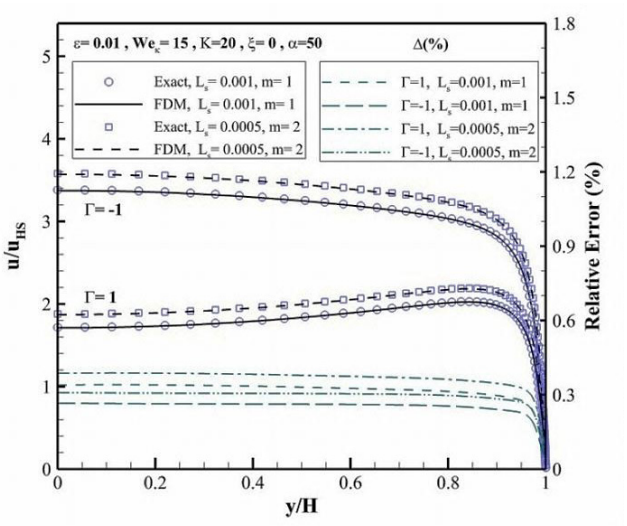

Fig. 3. Comparison between the results of the velocity profile in the mid-cross sectional plane of microchannel obtained from the present study with those in Ref. [1]

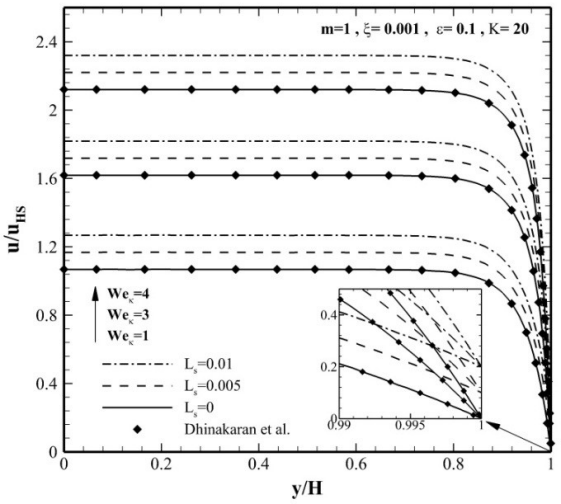

Fig. 4. One dimensional velocity profiles of axial electroosmotic flow, lines: present study, symbols: results of Ref. [25]

and y directions, respectively. In Table 1, the results of grid dependency study with respect to the volumetric viscoelastic fluid flow rate are provided at two different values of parameter ξ, two values of the Weissenberg number We_κ and various grid sizes applied on the computational plane. As can be seen, the minimum number of grids that satisfies the maximum truncation error of 10^{-4} with respect to volumetric flow rate is 70×70, and further increasing grid numbers does not significantly change the results of the FDM simulation for the volumetric flow rate.

It is noted that, due to decreasing the effect of channel aspect ratio on velocity profile at higher values of this parameter, we use α=1 as a critical value for grid dependency study. The reason of decreasing the effect of channel aspect ratio on flow dynamics at higher ranges of this parameter can be interpreted as follows; at large values of α, the variation of velocity profile at x direction is confined in the regions inside the EDL where the fluid is almost entirely affected by electroosmotic body force, and outside the EDL region, the fluid is more excited by the pressure driving force which results in a nearly parabolic shape velocity profile in the central regions of the microchannel. Therefore, it can be concluded that, by increasing α, the amount of curvature of the velocity profile in the x direction outside of the EDL decreases, and further increasing the number of grids for approximating the velocity profile outside of the EDL is not necessary. On the other hand, according to the plots of numerical method validation sketched in Fig. 3, by using the value of β=1.05 for stretching parameter, it is possible to simulate the viscoelastic fluid flow with reasonable accuracy even at large aspect ratios, i.e., α=50. Therefore, it can be said that, by using 150×150 grid numbers at the regions $1 \le \alpha \le 50$, both the grid independent results and flow simulations with a quality higher than that for 70×70 grid numbers is obtained.

7- Stability analysis for numerical and analytical methods

In this section, the stability analysis of the solutions is carried out in two aspects: 1. the stability of grid network, 2. the stability of viscoelastic fluid flow. The first case belongs to the FDM numerical simulation, and for increasing the stability of the numerical method and avoiding divergence in the iterative algorithm, an under relaxation factor, R_f is used and is defined as $u^2=R_f u^1+(1-R_f)u^0$ where u^0 and u^1 are the values of velocities at the grid points in two successive iterations, by which the value of velocity for each grid point in the network is calculated for using in the next iteration.

Also, for the latter case, the domain of stability of viscoelastic fluid flow in the analytical solution at various Weissenberg numbers and flow parameters is examined and compared with the results of FDM simulations at very low under relaxation factor R_f in 150×150 grid numbers. It is noted that, in the analytical solution, the range of operating parameters should be determined such that the Eq. (22) is integrable. Therefore, the sufficient condition for the integrability of this equation can be found as follows:

$$a^2 \mathrm{We}_\kappa^2 \left(\frac{\Gamma}{K} \bar{y} - \frac{\sinh K\bar{y}}{\cosh K} \right)^2 \le 1 \qquad (27)$$

According to Eq. (21), the left hand side of the above equation is the square of the dimensionless shear stress, $\bar{\tau}_{yz}^{\,2}$, which the value of that at $\Gamma \in (-\infty, K^2]$ becomes maximum at the channel walls. It is worthy to note the upper limit of Γ equal to K^2

Table 1. Grid dependency study of the present problem with respect to dimensionless volumetric flow rate ($\bar{Q}$)

Grid numbers	We_κ=3		We_κ=6	
	ξ=0	ξ=0.001	ξ=0	ξ=0.001
20×20	-0.964209	0.971644	1.141064	1.192010
30×30	0.964456	0.971948	1.142881	1.194346
40×40	0.964469	0.972005	1.143467	1.195131
50×50	0.964488	0.972609	1.143684	1.195434
60×60	0.964493	0.972902	1.143735	1.195473
70×70	0.964495	0.972908	1.143791	1.195489

is evaluated from the extremum of Eq. (21) for the cases of adverse pressure gradients. Therefore, for a certain value of the other parameters, the critical Weissenberg number, $We_{\kappa,c}$, can be obtained as follows:

$$\left|\mathrm{We}_{\kappa,c}\right| \le \frac{1}{a\left|\frac{\Gamma}{K} - \tanh K\right|} \qquad (28)$$

Therefore, it can be said that: 1. For small values of the EDL thickness relative to the half-height of the microchannel (K>>1), the hyperbolic term in the above equation approaches unity; 2. In the case of zero pressure gradient (Γ=0), the obtained relation by Dhinakaran et al. [25] for the critical Weissenberg number ($|We_{\kappa,c}| \le a^{-1}$) is recovered. Thus, the above relation for critical Weissenberg number is the extension of that by Dhinakaran et al. [25] in the stable domain of viscoelastic fluid flow for various values of pressure gradient, EDL thickness and the model parameter ξ. In Fig. 5, the variation of critical Weissenberg number with respect to parameter ξ at different values of velocity scale ratio is plotted. In this figure, the lines indicate the aforementioned variation obtained from Eq. (28) from the theoretical analysis, such that, for the Weissenberg number upper the lines of Fig. 5, there is not any real solution for 1D velocity profile. Also, to prove the correctness of Eq. (28), the FDM numerical simulation in some points through the plot of Fig. 5 is used to test the stability of the obtained solution.

The results of stability analysis from the FDM simulations is obtained under the conditions of microchannels with the large aspect ratios, i.e., α=20, $We_\kappa = We_{\kappa,c} \pm 0.5$ and 150×150 grid numbers at two different values of R_f=0.1,0.5. The obtained results implies a deterministic and stable velocity distribution for $We_{\kappa,c}$-0.5, however, for $We_{\kappa,c}$+0.5 even at very small under relaxation factor, the flow simulation with FDM does not converge. This phenomenon may imply the occurrence of viscoelastic instability in transition from the Weissenberg numbers lower than $We_{\kappa,c}$ to those higher than this value. The consequence of such transition may be interpreted as follows: the appearance of 3D-time dependent, chaotic flow whose simulation with the simplified assumptions employed in this problem is impossible. Therefore, in order to investigate this phenomenon, an unsteady and 3D flow analysis in a very refined grid network by direct numerical simulation methods should be conducted to represent the unstable behavior of viscoelastic fluids at high Weissenberg numbers.

8- Results and Discussion

In this section, at first, by using the theoretical analysis for velocity distribution of electroosmotic flow, the shear thinning effect of viscoelastic fluids in the presence of hydrophobic

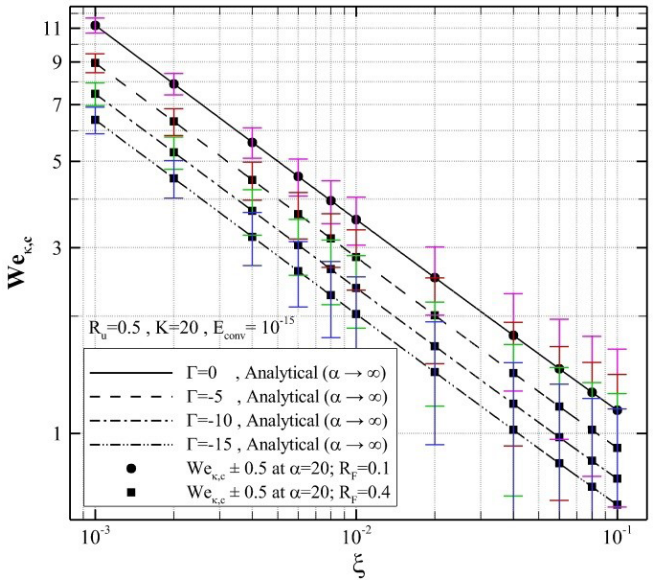

Fig. 5. Variation of critical Weissenberg number with respect to parameter ξ at different values of velocity scale ratio obtained from analytical and numerical study

properties of channel wall surfaces is investigated. In Fig. 4, the effects of Weissenberg number at three distinct values of We_{κ}=1,3 and 4 and constant values of model parameters ε and ξ were studied. As seen, increasing the value of We_{κ} causes an increase in the shear thinning effect associated with this parameter, and as a consequence, the maximum axial and bulk velocities are increased. Also, it is evident from this figure that, by increasing the amount of slippage in fluid-wall interface, i.e., increase in $\bar{L}_s$, a significant deviation from the assumption of no-slip boundary conditions at the walls emerges, such that, the change in the velocity profile due to increasing $\bar{L}_s$ is on the order of 0.1 maximum axial velocity.

In Fig. 6, the effect of uniaxial extensional viscosity predicted by the PTT viscoelastic model at different values of L_s is investigated. As can be seen, at constant values of Weissenberg number, parameter ξ and other electrokinetic parameters, the velocity plateau significantly increases by increasing parameter ε. However, at very small values of Weissenberg number for the present case of incompressible flows, the aforementioned parameter does not have a prominent effect on velocity profile. Also, in each velocity profile of electroosmotic flow, by increasing $\bar{L}_s$ at each value of extensional viscosity, the magnitude of velocity at the entire channel cross-section increases.

Fig. 7 shows the effect of parameter ξ on velocity profile at constant values of electrokinetic and viscoelastic parameters and in the presence of hydrophobicity. In this figure, for three cases of ξ=0.001,0.005 and 0.01, three distinct values of $\bar{L}_s$=0,0.001 and 0.002 are considered. Parameter ξ which reflects the non-affine motion of the polymeric network junctions relative to the continuum medium [19] is in the lower range of variation than other two model parameters, ε and We_{κ}. Therefore, the extent of effectiveness of this parameter on velocity profile is smaller than that of the two other parameters. From Fig. 7, it can be concluded that the effect of the Navier slip coefficient, $\bar{L}_s$, on velocity profile is much larger than that of parameter ξ under the same conditions; such that, by increasing $\bar{L}_s$ from 0 to 0.0002 at the slip exponent of 3, the amount of bulk velocity profile increases up to two fold. In a comparison between Figs. 6 and 7, at larger values of slip exponent, the amount of fluid-wall slippage increases more with changing $\bar{L}_s$, such that, we can see from these two figures that at m=2, the effect of $\bar{L}_s$ on velocity profile is much smaller than that in m=3.

In this step, the results of the FDM numerical simulation for 2D velocity distribution in the cross section of the microchannel are investigated. For this case, in order to consider the fluid-wall slippage, we use the values of m=2 and $\bar{L}_s$=0.0005 at the channel wall surfaces. In Fig. 8, the two dimensional velocity profile for α=1 and in the presence of favorable pressure gradient is illustrated. We can see the effect of pressure gradient in the same direction of electroosmotic force on the generation of convex velocity profile at the entire cross section of microchannel. Also, from this velocity profile, the uniform increasing effect of slip boundary conditions on velocity distribution even at the regions far from the walls can be seen. However, due to larger hydrodynamic resistance, the effect of slip boundary conditions at the corners of microchannel is much smaller than the regions far from the edges of the microchannel.

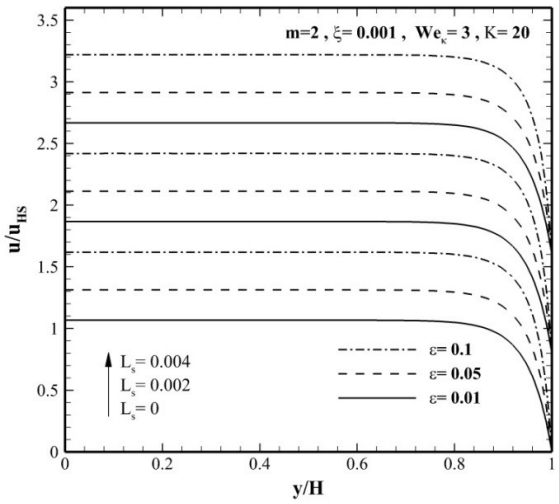

Fig. 6. The velocity profiles of electroosmotic flow in the mid-cross sectional plane at various $\bar{L}_s$ and ε

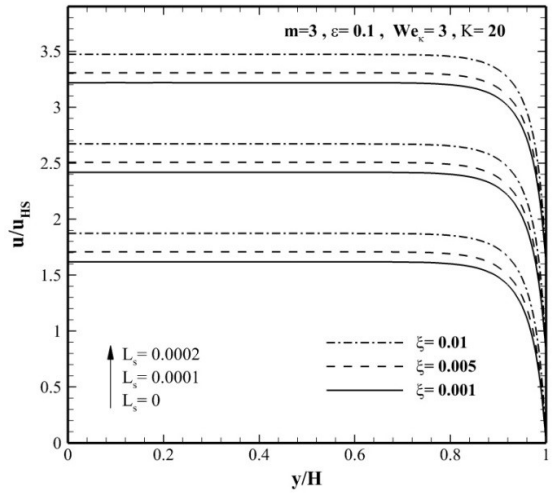

Fig. 7. The velocity profiles of electroosmotic flow in the mid-cross sectional plane at various $\bar{L}_s$ and ξ

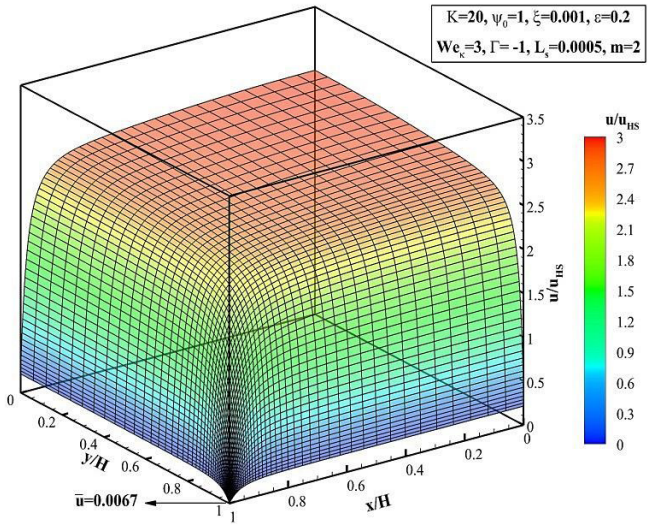

Fig. 8. 2D velocity profile of electroosmotic flow of PTT fluid in the case of favorable pressure gradient (Γ= -1)

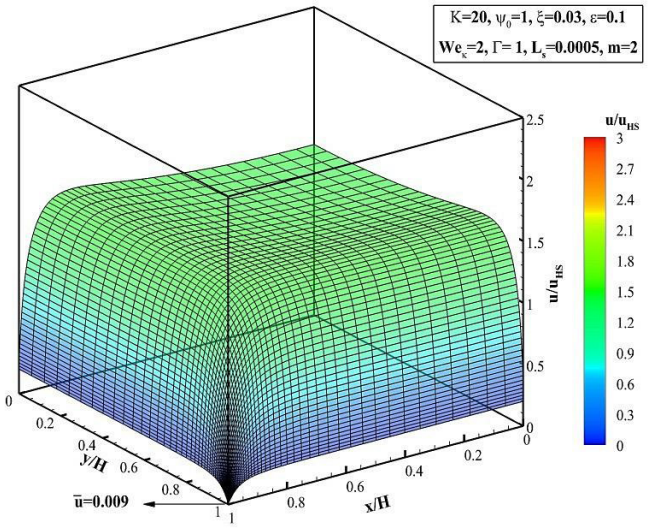

Fig. 9. 2D velocity profile of electroosmotic flow of PTT fluid in the case of adverse pressure gradient (Γ= 1)

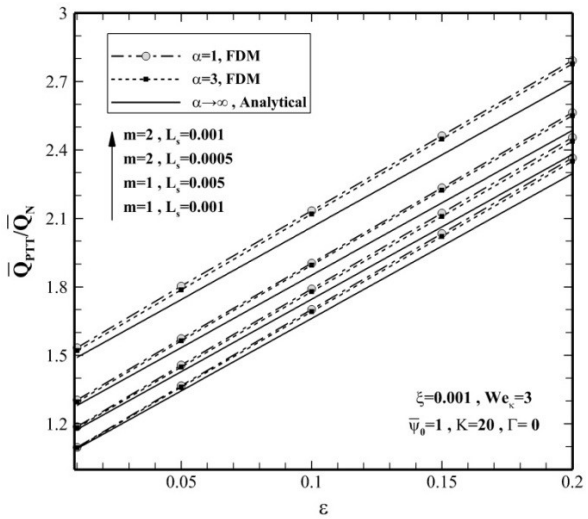

Fig. 10. Variation of ratio of dimensionless viscoelastic to Newtonian volumetric flow rate with respect to ε at various α

In Fig. 9, the mixed electroosmotic and pressure opposed flows of viscoelastic fluids at α=1 and in the presence of the surface hydrophobicity at the upper right quadrant of the channel cross section are shown. To plot this figure, the pressure driven flow control parameter is set to Γ=1 which denotes that the characteristic value of pressure driven flow velocity in the reverse direction relative to the electroosmotic flow is in the same magnitude as compared with the Helmholtz–Smoluchowski velocity. As can be seen from this figure, there is a non-uniform velocity distribution in the cross section of the microchannel; such that, at the regions far from the channel walls, the electrokinetic effects of dielectric channel walls is much smaller than the regions inside the EDL, and therefore, the velocity profile is nearly concave at the central regions while is convex at the areas near the walls. In this flow scenario, due to increasing the hydrodynamic resistance of the channel geometry at the corners, the extent of fluid-wall slippage is reduced in these areas while by increasing the shear rate in the middle regions of the channel walls, the amount of fluid-wall slippage is observable.

As discussed in introduction of this study, due to the large surface area-to-fluid volume ratio in microfluidic devices, the use of hydrophobic materials results in an improvement of the rate of fluid flow in these systems. In Fig. 10, the variation of the ratio of volumetric flow rate of viscoelastic fluids to that of Newtonian fluids with respect to the model parameter ε at two different values of α=1 and 3 and various values of slip parameters obtained from FDM simulations are plotted. It is noted that the volumetric flow rate of Newtonian fluids is calculated under the no-slip boundary conditions. Also, the variation of the aforementioned ratio for slit microchannels, i.e., $\alpha\rightarrow\infty$, is calculated from the analytical solution, and the relevant results are shown in this figure.

As can be seen in Fig. 10, at low values of ε in which the deviation of rheology behavior of the PTT model at a small value of ξ=0.001 relative to UCM model is not significant, the effect of slip velocity on increasing the volumetric flow rate relative to the Newtonian model is negligible. However, for higher values of model parameter ε, and simultaneously, increasing the shear thinning effect of PTT fluids associated with this parameter, the influence of Navier slip coefficient on increasing the volumetric flow rate is more dramatic than that for the low values of parameter ε. Also, it can be seen from this figure that, by increasing the channel aspect ratio, the amount of deviation of viscoelastic fluid flow rate from its Newtonian counterpart is reduced. The reason of this change is that, as the channel aspect ratio increases, the magnitude of velocity gradient due to the electrokinetic effects of channel walls at the vast central region of the microchannel decreases, and consequently, by decreasing the strain rate of the viscoelastic fluid, on the rheological behavior of the PTT fluids has less influence on the variation of volumetric flow rate.

9- Conclusion

In this paper, we presented a numerical study of mixed electro-osmotic/Poiseuille slip flow of viscoelastic fluids in microchannels with rectangular cross sections. In this regard, the complete form of the PTT-constitutive equation was used to describe the rheological behavior of the fluid. A second order finite difference method was employed to investigate the 2D velocity distribution and volumetric flow rate in the

presence of wall surface hydrophobicity through rectangular microchannels. The numerical results being validated by the same simplified theoretical study of the literature revealed an excellent accuracy with a relative error less than 0.3%. Also, the exact solution of electroosmotic flow of PTT-viscoelastic fluids was derived for slit hydrophobic microchannels, and after validating, the solution was used to capture the rheological behavior of PTT fluids in the range of operating parameters.

In this investigation, by considering the fluid-wall slippage at channel walls with hydrophobic surfaces, the effect of Navier slip coefficient in various values of slip exponent was interrogated. In this regard, the variation of 1D and 2D velocity profiles obtained from theoretical and numerical analysis, respectively, at different Navier slip coefficients and different values of viscoelastic parameters were shown. The results of velocity distribution at three different flow scenarios of zero, adverse, and favorable pressure gradients were analyzed, which a dramatic shear thinning effect of extensibility parameter and the Weissenberg number on the shear thinning behavior of PTT fluids was illustrated. However, the aforementioned change in the dynamics of PTT fluid due to the variation of model parameter ξ was much smaller than two other parameters. Also, the quantitative investigation of the Navier slip coefficient on volumetric flow rate of viscoelastic fluid normalized with the Newtonian counterpart exhibited; 1. a small deviation of PTT fluid flow characteristics relative to the flow of UCM model fluids at low values of extensibility parameter, and 2. a salient influence of slip coefficient on volumetric flow rate at higher values of model parameter ε. On the other hand, the results of this study revealed that the shear thinning effect of parameter ε on increasing the amount of viscoelastic volumetric flow rate normalized with the Newtonian counterpart is more prominent at low channel aspect ratios.

Acknowledgement

The research chair of novel energy conversion systems at Sharif University of Technology (SUT) and Iran National Science Foundation (INSF) are highly acknowledged for their financial support.

Nomenclature

A	Coefficients in discretized equations
D	The rate of strain tensor, s^{-1}
e	Electron charge, $=1.6\times10^{-19}$ C
E_z	Axial electric field, $V.m^{-1}$
$f(\tau_{kk})$	Stress coefficient function
$\mathbf{F},F_z$	Total/electric body force, N
k_B	Boltzmann constant,$=1.38\times10^{-23}$ JK^{-1}
K	Dimensionless Debye-Hückel parameter
L,H,W	Length, height and width, m
n_0	Ionic number concentration, m^{-3}
Q	Volumetric flow rate, $m^3.s^{-1}$
p	Pressure, Pa
Re	Reynolds number
T_m	The absolute mean temperature of the fluid, K
$\boldsymbol{u},u$	Velocity vector/axial velocity, $m.s^{-1}$
u_{HS}	Helmholtz-Smoluchowski velocity, ms^{-1}
We_κ	Weissenberg number
x,y,z	Stream-wise, depth-wise and axial directions

Greek symbols

α	The ratio of channel width to height
β	Stretching parameter
ε	The extensional viscosity of PTT fluid
ϵ	Permittivity of electrolyte
Γ	Velocity scale ratio
η_p	Polymeric viscosity coefficient (Pa.s)
κ	Debye-Hückel parameter (m^{-1})
λ	Fluid relaxation time (s)
τ_{kk}	Trace of extra stress tensor
τ	Extra polymeric stress tensor (Pa)
ψ,ψ_0	Electrical/wall-zeta potential (V)
z	Ionic valence

subscripts

ψ,u	Electrical potential/velocity
P,NB	Central, neighboring grid points
c	Source term
i,j,k	Grid indices

superscripts

-	Dimensionless parameter
^	Transformed-dimensionless parameter

References

[1] A. Afonso, L. Ferrás, J. Nóbrega, M. Alves, F. Pinho, Pressure-driven electrokinetic slip flows of viscoelastic fluids in hydrophobic microchannels, *Microfluidics and nanofluidics*, 16(6) (2014) 1131-1142.

[2] F. Brochard, P. De Gennes, Shear-dependent slippage at a polymer/solid interface, *Langmuir*, 8(12) (1992) 3033-3037.

[3] Y. Inn, S.-Q. Wang, Hydrodynamic slip: Polymer adsorption and desorption at melt/solid interfaces, *Phys. Rev. Lett.*, 76(3) (1996) 467.

[4] K. Migler, H. Hervet, L. Leger, Slip transition of a polymer melt under shear stress, *Phys. Rev. Lett.*, 70(3) (1993) 287.

[5] V. Marry, J.-F. Dufrêche, M. Jardat, P. Turq, Equilibrium and electrokinetic phenomena in charged porous media from microscopic and mesoscopic models: electro-osmosis in montmorillonite, *Molecular Physics*, 101(20) (2003) 3111-3119.

[6] A. Herr, J. Molho, J. Santiago, M. Mungal, T. Kenny, M. Garguilo, Electroosmotic capillary flow with nonuniform zeta potential, *Anal. Chem.*, 72(5) (2000) 1053-1057.

[7] H.A. Stone, A.D. Stroock, A. Ajdari, Engineering flows in small devices: microfluidics toward a lab-on-a-chip, *Annu. Rev. Fluid Mech.*, 36 (2004) 381-411.

[8] M. Gad-el-Hak, The fluid mechanics of microdevices—the Freeman scholar lecture, *Journal of Fluids Engineering*, 121(1) (1999) 5-33.

[9] Y.L. Zhang, R.V. Craster, O.K. Matar, Surfactant driven flows overlying a hydrophobic epithelium: film rupture in the presence of slip, *J. Colloid Interface Sci.*, 264(1) (2003) 160-175.

[10] D.J. Beebe, G.A. Mensing, G.M. Walker, Physics and applications of microfluidics in biology, *Annual review of biomedical engineering*, 4(1) (2002) 261-286.

[11] J.C. Maxwell, On stresses in rarified gases arising from inequalities of temperature, *Philosophical Transactions of the royal society of London*, 170 (1879) 231-256.

[12] Y. Zhu, S. Granick, Rate-dependent slip of Newtonian liquid at smooth surfaces, *Phys. Rev. Lett.*, 87(9) (2001) 096105.

[13] V.S. Craig, C. Neto, D.R. Williams, Shear-dependent boundary slip in an aqueous Newtonian liquid, *Phys. Rev. Lett.*, 87(5) (2001) 054504.

[14] C. Soong, P. Hwang, J. Wang, Analysis of pressure-driven electrokinetic flows in hydrophobic microchannels with slip-dependent zeta potential, *Microfluidics and Nanofluidics*, 9(2-3) (2010) 211-223.

[15] J. Jamaati, H. Niazmand, M. Renksizbulut, Pressure-driven electrokinetic slip-flow in planar microchannels, *International Journal of Thermal Sciences*, 49(7) (2010) 1165-1174.

[16] C. Navier, Mémoire sur les lois du mouvement des fluides, *Mémoires de l'Académie Royale des Sciences de l'Institut de France*, 6 (1823) 389-440.

[17] D.C. Tretheway, C.D. Meinhart, Apparent fluid slip at hydrophobic microchannel walls, *Phys. Fluids*, 14(3) (2002) L9-L12.

[18] B.-H. Jo, L.M. Van Lerberghe, K.M. Motsegood, D.J. Beebe, Three-dimensional micro-channel fabrication in polydimethylsiloxane (PDMS) elastomer, *Journal of Microelectromechanical Systems*, 9(1) (2000) 76-81.

[19] N. Phan-Thien, A nonlinear network viscoelastic model, *J. Rheol.*, 22(3) (1978) 259-283.

[20] N.P. Thien, R.I. Tanner, A new constitutive equation derived from network theory, *J. Non-Newtonian Fluid Mech.*, 2(4) (1977) 353-365.

[21] D. Li, Electrokinetics in microfluidics, *Academic Press*, 2004.

[22] M. Chatzimina, G.C. Georgiou, K. Housiadas, S.G. Hatzikiriakos, Stability of the annular Poiseuille flow of a Newtonian liquid with slip along the walls, *J. Non-Newtonian Fluid Mech.*, 159(1) (2009) 1-9.

[23] R.H. Pletcher, J.C. Tannehill, D. Anderson, Computational fluid mechanics and heat transfer, *CRC Press*, 2012.

[24] A. Afonso, M. Alves, F. Pinho, Analytical solution of mixed electro-osmotic/pressure driven flows of viscoelastic fluids in microchannels, *J. Non-Newtonian Fluid Mech.*, 159(1) (2009) 50-63.

[25] S. Dhinakaran, A. Afonso, M. Alves, F. Pinho, Steady viscoelastic fluid flow between parallel plates under electro-osmotic forces: Phan-Thien–Tanner model, *J. Colloid Interface Sci.*, 344(2) (2010) 513-520.

Please cite this article using:

M. Reshadi and M. H. Saidi, "Investigation of Mixed Electro-Osmotic/Poiseuille Slip Flows of Viscoelastic Fluids in Rectangular Microchannels with Hydrophobic Surfaces", *AUT J. Mech. Eng.*, 1(1) (2017) 3-12.

DOI: 10.22060/mej.2016.715